Geophys. J. Int. (2010) **181,** 99–112 doi: 10.1111/j.1365-246X.2009.04482.x

Post-seismic and interseismic fault creep II: transient creep and interseismic stress shadows on megathrusts

E. A. Hetland[1] and M. Simons[2]

[1] *Department of Geological Sciences, University of Michigan, Ann Arbor, MI, USA. E-mail: ehetland@alum.mit.edu*
[2] *Seismological Laboratory, California Institute of Technology, Pasadena, CA, USA*

Accepted 2009 December 12. Received 2009 October 8; in original form 2009 Marh 22

SUMMARY

We use idealized subduction megathrust models to examine aseismic, frictional fault creep throughout the interseismic period. We consider rate-dependent and rate- and state-dependent friction. When there is significant post-seismic creep surrounding locations of coseismic slip, the creep rates surrounding an asperity may be lower than the plate convergence rate late in the seismic cycle. This lowering of the creep rates is due to stress shadows forming around the interseismically locked asperities. The size of the stress shadows increases as there is more transient post-seismic creep. Larger asperities produce larger interseismic stress shadows, and multiple asperities can act together to produce a stress shadow larger than the sum of the effects of the individual asperities. For rate-state frictional megathrusts, there is a wide range of transient post-seismic creep that occurs: from pulses of post-seismic creep with decreasing creep rates through time, to delayed post-seismic creep. Delayed post-seismic creep may occur well into the interseismic period, with transient creep lasting over a significant portion of the seismic cycle. Delayed post-seismic creep is generally favoured in velocity strengthening regions with either a larger magnitude of the frictional direct effect or a larger effective normal stress. In addition, regions of the fault undergoing delayed post-seismic creep must be above steady state following coseismic slip.

Key words: Seismic cycle; Rheology and friction of fault zones; Subduction zone processes; Dynamics and mechanics of faulting.

1 INTRODUCTION

In 1983, J. Savage proposed the kinematic backslip model of interseismic deformation in subduction zones (Savage 1983). This backslip model was motivated by an equivalent model of interseismic deformation near continental strike slip faults (Savage & Burford 1973), and describes interseismic deformation through imposed fault slip in an elastic half-space. The name of the model derives from its assumption that in the hanging wall interseismic deformation must cancel coseismic deformation, and thus interseismic deformation is identical to locked regions slipping opposite to the sense of the megathrust loading (i.e. backslip). The backslip model is most commonly used in studies of strain accumulation on megathrusts (e.g. Nishimura *et al.* 2004; Norabuena *et al.* 2004), where regions of high backslip rates roughly correspond to asperities (e.g. Bürgmann *et al.* 2005; Suwa *et al.* 2006; Hashimoto *et al.* 2009). Asperities are generally defined to be regions of coseismic slip (e.g. Aki 1984; Kanamori 1986; Bilek & Lay 2002), although in this paper we use 'asperities' to refer to regions that only experience coseismic slip, with negligible interseismic creep (we use 'creep' to specifically refer to aseismic fault slip). We use "transition regions" to refer to those regions of the fault adjacent to asperities that both slip during earthquakes and creep during the interseismic period. The backslip model is entirely kinematic, and thus there is no explicit connection between backslip and the mechanical properties of the megathrust. Most researchers acknowledge that the backslip model merely captures the instantaneous creep rate of the megathrust (e.g. Mazzotti *et al.* 2000; Nishimura *et al.* 2004), although backslipping regions are often referred to as coupled. Wang & Dixon (2004) and Wang (2007) argue that an over-reliance on coupling concepts in the backslip model can lead to several physical inconsistencies, mostly arising due to the lack of a megathrust rheology in this kinematic model. Kanda & Simons (2009) showed that by accounting for the full deformation field of the slab as it bends through the subduction system, the backslip methodology can apply to non-planar faults as long as the slab bending stresses are relieved continuously during the earthquake cycle, or the stresses due to the bending of the plate are negligible.

In almost all subduction zones where the backslip model has been applied, regions of large inferred coupling are much broader and smoother than the known locations of past earthquakes (e.g. Nishimura *et al.* 2004; Suwa *et al.* 2006; Chlieh *et al.* 2008). The smoothness of backslip is partly due to an imposed regularization in the backslip model. Bürgmann *et al.* (2005) used the

locations of known asperities to decrease the artificial smoothness of the backslip model, and suggested that coseismic slip may occur on fully locked asperities surrounded by partially coupled regions. There also may be mechanical reasons for smooth variations in the degree of apparent coupling resolved in a backslip model. For instance, it has been suggested that partially coupled regions (i.e. regions with non-zero backslip less than the plate rate) may indicate numerous small asperities (Igarashi *et al.* 2003), or regions experiencing long-lived transient slow slip (Meade & Loveless 2009). In addition, if the total post-seismic creep following a megathrust earthquake is comparable to the coseismic slip, then large regions surrounding the asperities may creep slower than plate rate at the end of the interseismic period, appearing partially coupled within a backslip formulation (e.g. Savage 1995; Mazzotti *et al.* 2000; Nishimura *et al.* 2004).

In contrast to the steady interseismic creep observed during the later interseismic period, creep following large earthquakes tends to be highly transient. Observed transient post-seismic creep on megathrusts exhibits a spectrum of behaviours from relatively simple decay of initially large post-seismic creep rates (e.g. Heki *et al.* 1997; Miyazaki *et al.* 2004; Hsu *et al.* 2006), to a complicated interaction between propagating post-seismic creep and large aftershocks (e.g. Yagi *et al.* 2003; Miura *et al.* 2006; Pritchard & Simons 2006). We do not investigate the complex interaction between post-seismic creep and aftershocks; however, we show that in models with frictional faults, post-seismic creep rates do not always decay from large rates immediately following an earthquake. For example, for some rate-state, velocity strengthening friction faults, post-seismic creep rates following coseismic slip may be initially low, and then increase later in the interseismic period, before decreasing back below the plate convergence rate. We refer to this as delayed post-seismic creep, and the delay of the transient creep may be significant relative to the recurrence time between large earthquakes. The delayed post-seismic creep we explore is similar to the unstable transient creep explored by Perfettini & Ampuero (2008) and Helmstetter & Shaw (2009).

We use the model of localized fault creep we developed in a companion paper (Hetland, Simons, & Dunham 'Interseismic and post-seismic Fault Creep I: Model Description'; hereafter referred to as Paper I), to illustrate some of the interseismic creep behaviour one might expect for a heterogeneous megathrust frictional rheology. Specifically, we first demonstrate that late in the seismic cycle, interseismic creep rates surrounding asperities can be much less than the plate convergence rate, due to the fact that interseismically locked asperities shadow stresses on the surrounding megathrust late in a seismic cycle. The pattern of these stress shadows depends on the megathrust rheology and the configuration of the asperities. Second, we explore a few ways in which spatial heterogeneity of the megathrust rheology affects transient creep rates throughout the interseismic period. We do not attempt to explore the infinite combination of asperity geometries and heterogeneous megathrust rheologies. Instead, we present a few simplified models in order to build intuition about the relationship between interseismic creep and megathrust rheology.

2 MODEL CONSTRUCTION

We consider an idealized megathrust geometry throughout this paper, composed of a reverse fault dipping 20° from horizontal (Fig. 1a). We only calculate fault slip in the thrust direction, and all results we present are the thrust-component. We do not describe the model calculation here, and refer readers to Paper I for details of the model formulation. The computational domain is $20D$ along strike and $10D$ along dip, where D is a characteristic dimension of asperities (see Table 1 for list of model symbols; Fig. 1a). The fault is assumed to slide steadily at the plate convergence rate, v_T, outside of the computational domain. The size of the computational domain is chosen in order to minimize the effect of the boundary conditions, since when the fault boundaries are relatively close to the asperities, the creep rates late in the seismic cycle can be artificially high due to the proximity of the boundary conditions (see Paper I, section 3.3). To limit the computational burden of these models, we use a uniform fault discretization from $-4D$ to $4D$ along strike and 0–$3.5D$ along dip, and a non-uniform discretization in the far-field (Fig. 1). The model is discretized into 6508 fault cells, and as of writing, on a desktop computer it takes roughly ten minutes to calculate the model kernels using Okada (1992) in Matlab. The kernels only need to be calculated once for each fault geometry, and require just under 1 GB of storage.

We impose all coseismic slip, and we assume that asperities slip uniformly, with coseismic slip arbitrarily tapering to zero outside of the asperity (Fig. 2; see Paper I, Section 3.2 for a discussion of coseismic slip in non-asperity regions). It is important to note that the exact pattern of coseismic slip depends on the frictional properties in both the velocity weakening regions and the adjacent velocity strengthening regions (e.g. Boatwright & Cocco 1996; Tinti *et al.* 2005; Hillers & Wesnousky 2008). Hence, as discussed in section 5.1 of Paper I and below, the imposed coseismic slip in the transition regions might be inconsistent with the frictional parameters we assume. We spin-up the models from the initial fault traction required to slide the fault steadily at v_T, and we apply coseismic slip

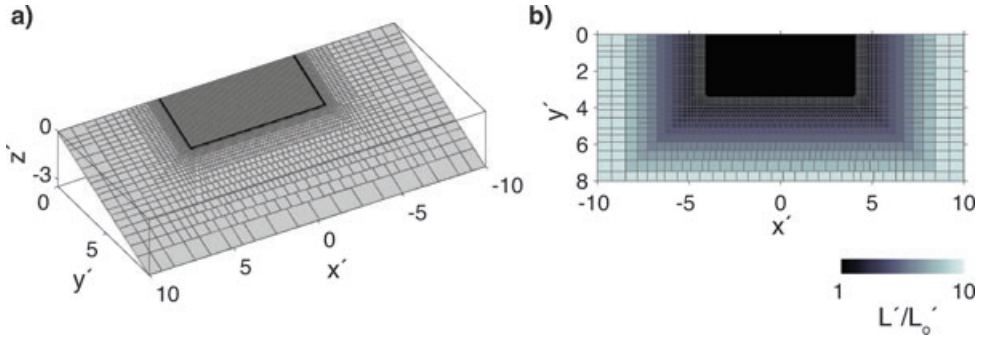

Figure 1. (a) Idealized megathrust model, grey lines show the fault discretization and black line outlines of the region of constant fault cell size. (b) Surface projection of central region of the fault, showing the variation of L' over the fault; for clarity, the fault discretization in the region of uniform mesh is not shown in (b).

Table 1. Definition of symbols used in main text.

a	Magnitude of the direct effect in friction
b	Magnitude of the evolution effect in friction
D	Characteristic model dimension
f	Fault friction
f_a	Critical fault friction for unstable creep
f_o	Reference fault friction
k	Fault stiffness
k_b	Critical fault stiffness for unstable creep
L	Characteristic slip distance in RS friction ($L' = L/s_o$)
L_b	Critical distance for unstable creep ($L'_b = L_b/D$)
s_o	Characteristic coseismic slip
t	Time ($t' = t/T$)
T	Characteristic earthquake recurrence time
v	Fault creep rate ($v' = v/v_T$)
v_T	$= s_o/T$, characteristic slip rate
α	$= a\sigma_E$ in RS friction ($\alpha' = a\sigma'_E$)
α_h	$=(a-b)\sigma_E$ in RD friction ($\alpha'_h = (a-b)\sigma'_E$)
γ	$= b/a$
μ	Shear modulus
Ω	$= v\theta/L$
ρ	$= f_o/a$ in RS friction
ρ_h	$= f_o/(a-b)$ in RD friction
σ_E	Effective normal stress across the fault ($\sigma'_E = \sigma_E\ D/\mu s_o$)
σ_o	Reference normal stress across the fault ($\sigma'_o = \sigma_o\ D/\mu s_o$)
τ	Traction on the fault ($\tau' = \tau\ D/\mu s_o$)
θ	RS friction state variable ($\theta' = \theta/T$)
ζ	General fault coordinates ($\zeta' = \zeta/D$)

Note: Non-dimensionalize parameters are denoted with a prime, and defined where appropriate.

periodically in time, with repeat time T and maximum slip s_o($v_T = s_o/T$). The model spins-up in a few seismic cycles, typically less than five, (see Paper I, Section 3.1 for a discussion of spin-up in these models), and we only present the seismic cycle invariant results from fully spun-up models. As of writing, spin-up takes from 20 min to an hour on a desktop computer, depending on the fault rheologies and the imposed coseismic slip, and the calculation of interseismic slip in Matlab requires just under 2 GB of memory. All models presented are non-dimensionalized and the non-dimensional variables are denoted with a prime (see Table 1 for non-dimensionalizations).

We focus on velocity strengthening frictional fault zones, with either rate-dependent friction or rate- and state-dependent friction, which we refer to as 'RD friction' or 'RS friction', respectively. The fault constitutive equation for RD friction is

$$v'(\zeta', t') = 2e^{-\rho_h(\zeta')} \sinh\left\{\frac{\tau'(\zeta', t')}{\alpha'_h(\zeta')}\right\}, \tag{1}$$

where we take v_T to be the frictional reference slip rate, and we define $\alpha'_h \equiv (a-b)\sigma'_E$ and $\rho_h \equiv f_o/(a-b)$, for reference friction f_o, frictional parameters a and b, and effective normal traction σ'_E (e.g. Marone *et al.* 1991, Paper I). The fault constitutive equation for RS friction is

$$v'(\zeta', t') = 2e^{-\rho(\zeta')} \sinh\left\{\frac{\tau'(\zeta', t')}{\alpha'(\zeta')}\right\}\left[\frac{\theta'(\zeta', t')}{L'(\zeta')}\right]^{-\gamma(\zeta')}, \tag{2}$$

where we again take v_T to be the frictional reference slip rate, $\alpha' \equiv a\sigma'_E$, $\rho \equiv f_o/a$, $\gamma \equiv b/a$, $L' = L/s_o$, L is the frictional characteristic slip distance, $\theta' = \theta/T$ is non-dimensional frictional state, and all other parameters are as defined above (e.g. Dieterich 1979; Ruina 1983). Our choice of terms to parametrize friction is motivated by Paper I, where we show that ρ_h and ρ or α_h and α affect interseismic creep in similar ways. α is the product of the magnitude of the frictional direct effect, a, and the normal stress on the fault, σ'_E, and γ is the ratio of the magnitudes of the evolution effect, b, to the direct effect in RS friction. We further note that eqs (1) and (2) do not depend separately on the parameters a, b, f_o and σ'_E.

We assume that frictional state varies according to the slip law, given by

$$\frac{\partial\theta'(\zeta', t')}{\partial t'} = 1 - \frac{\theta'(\zeta', t')|v'(\zeta', t')|}{L'(\zeta')} \tag{3}$$

(e.g. Marone 1998). For velocity strengthening friction, $(a-b) > 0$ or equivalently $\gamma < 1$. For reasonable values of frictional parameters and characteristic dimensions, ρ_h and ρ are about 10–100, α_h and α are of order 10^{-1}, and L' is about 10^{-7}–10^{-3}. In practice, calculations with L' this low are too computationally burdensome (see discussions in Rice 1993; Lapusta & Rice 2003, Paper I), and we take $L' > 10^{-2}$ for most of the models we consider.

For RD friction, except in Section 3, we assume homogeneous fault properties across the non-asperity regions of the megathrust, with $\rho_h = 10$ and variable α'_h. For RS friction, except in Section 3, we assume spatially homogeneous $\rho = 10$ and $\gamma = 0.9$. We vary α' in these models, and we mainly consider α' spatially uniform across the megathrust, although in Section 5 we consider a particular instance of heterogeneous α'. We assume constant $L' = L'_o$ in the centre of the megathrust where the fault discretization is constant, and we increase L' in the far field at the same rate that the along-dip cell dimension increases (Fig. 1b). This increase in L' arises because the local fault cell size limits the permissible RS friction parameters (Perfettini & Ampuero 2008); however, in all models we specify that L' in the far-field is ten times L'_o, regardless of whether a smaller L' in the far-field would be permissible. Interseismic creep in the far-field does not significantly deviate from steady creep during the entire calculation.

3 INTERSEISMIC VARIATION OF NORMAL TRACTION

The example models presented in Paper I, assumed infinite length, vertical strike-slip faults. In those models, normal traction across

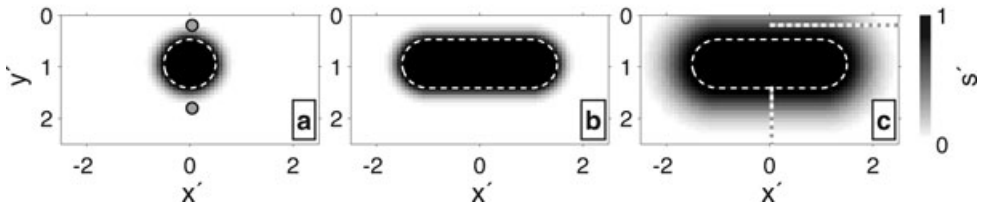

Figure 2. Surface projection of coseismic slip distributions considered in this paper, dashed line indicates the extent of the asperity. Circles in (a) are locations where creep rates are shown in Fig. 3, and black–grey stippled lines in (c) are transects along which interseismic creep rates are shown in Fig. 10.

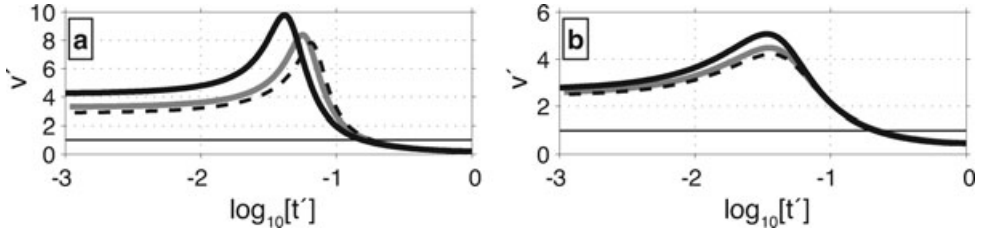

Figure 3. Interseismic creep rate at $y' = 0.2$ (a) and 1.8 (b) along the centre of models (see Fig. 2) with RS friction megathrusts, where the variation in normal traction is either ignored (dashed lines) or accounted for (solid lines) in the calculation of interseismic creep; thin solid line is $v' = 1$. In the model where variable normal traction is ignored, $\alpha' = 0.3$ and $\rho = 13.33$ (grey dashed lines; lines are overprinted by black dashed lines) or 40 (black dashed lines), and in the model where normal traction is accounted for, $a = 0.0150$, $\sigma'_{\rm o} = 20$, and $f_{\rm o} = 0.2$ (grey solid lines) or 0.6 (black solid lines); $\gamma = 0.9$ and $L' = 0.06$ in all models.

the faults did not vary during the interseismic period. Both coseismic and interseismic slip, either strike-slip or dip-slip, on a finite portion of a dipping fault will lead to variations in normal traction, and these variations may be significant, particularly in subduction zones (e.g. Wang & He 2008). In general, any slip on an arbitrarily shaped fault leads to variations in normal traction across that fault. Coseismic slip leads to larger perturbations of fault normal traction compared to interseismic creep, because of the larger fault offsets. At noted in Paper I, we can include time-dependent normal traction in the frictional fault constitutive equations by setting $\sigma'_E(\zeta', t') = \sigma'_{\rm o}(\zeta') + \tau'_n(\zeta', t')$, where $\sigma'_{\rm o}(\zeta')$ is a non-dimensional reference normal traction, and $\tau'_n(\zeta', t')$ is the time-dependent normal traction. As long as $\sigma'_{\rm o}(\zeta') \gg \tau'_n(\zeta', t')$, the variation of normal traction can be ignored in the frictional constitutive equations. However, if $\tau'_n(\zeta', t')$ is of order of, or greater than, $\sigma'_{\rm o}(\zeta')$, the variation of normal traction needs to be accounted for. When we include variations in normal traction in the fault constitutive equations, it is no longer convenient to parametrize RS friction by ρ, γ, and α' (ρ_h and α'_h for RD friction), and instead it is more natural to consider a, b, $f_{\rm o}$ and $\sigma'_{\rm o}(a - b)$, $f_{\rm o}$ and $\sigma'_{\rm o}$ for RD friction).

We demonstrate the effect of including variations in normal traction using our megathrust model with an RS friction rheology and the coseismic slip distribution in Fig. 2(a). We consider four RS friction models, two including $\tau'_n(\zeta', t')$ and two assuming $\sigma'_E = \sigma'_{\rm o}$ (for simplicity we assume a uniform $\sigma'_{\rm o}$ across the megathrust). We refer to the former models as 'variable normal traction' (VNT) models, and the latter as the 'constant normal traction' (CNT) models. In all four models, we set $\gamma = 0.9$ and $L'_{\rm o} = 0.06$. In the two VNT models, we take $a = 0.0150$, $b = 0.0135$, $\sigma'_{\rm o} = 20$ and $f_{\rm o} = 0.2$ (VNT model 1) or 0.6 (VNT model 2). In the two CNT models, we take $\alpha' = 0.3$ and $\rho = 13.33$ (CNT model 1) or 40 (CNT model 2). Note that if $\tau'_n(\zeta, t) = 0$, VNT model 1 and CNT model 1 are identical and VNT model 2 and CNT model 2 are identical.

For simplicity, we only compare the spun-up model results at two points, one updip of the asperity, and one downdip of the asperity (Fig. 2a). Due to the weak dependence of the interseismic creep on changes in ρ in these models (see Section 4.2 of Paper I), the interseismic creep rates at the two locations in CNT models 1 and 2 are virtually identical (Fig. 3). However, the interseismic creep rates in the two VNT models are distinct from those in the CNT models (Fig. 3). The effect on the creep rate of including variable normal traction is greatest updip of the asperity, where coseismic slip causes a larger decrease in normal traction (Fig. 3). In addition, the change in interseismic creep rate is greater when $f_{\rm o} = 0.6$ compared to when $f_{\rm o} = 0.2$ (Fig. 3). In these models, the coseismic normal traction perturbation is at most about 0.5, which is more than an order of magnitude smaller than the reference normal traction of 20. For a characteristic asperity size of 10 km, coseismic slip of 1 m, and shear modulus of 10 GPa, $\sigma'_{\rm o} = 20$ corresponds to $\sigma_{\rm o} = 20$ MPa. For lower $\sigma'_{\rm o}$, variations in normal traction influence the interseismic creep to a larger degree. As $\sigma'_{\rm o}$ increases beyond 20, time-dependent normal traction due to fault slip has an increasingly smaller effect on interseismic creep rate.

Creep rates in the CNT and VNT models are only different during the early interseismic period (Fig. 3). The increased rates in the VNT models are partially offset by decreased rates later in the interseismic period, and thus there is little effect on the cumulative creep later in the interseismic period. For the rest of the calculations in this paper, we ignore any time-dependence in normal traction on the megathrust. We do this mainly to decrease the number of controlling parameters in the frictional constitutive equations, especially since many of them are not well constrained *a priori*. It should be understood, that the effect of ignoring time-dependent normal traction could change the predicted post-seismic creep rates, although the general relationships that we illustrate in this paper hold whether we include time-dependent normal traction or we do not. When not including the variation of fault normal traction, we use γ, ρ and α to parametrize RS friction (ρ_h and α_h in RD friction), as our model is not sensitive to $f_{\rm o}$, a, b or σ'_E individually.

4 INTERSEISMIC STRESS SHADOWS

For most frictional rheologies in our models, creep rates are high surrounding the asperity immediately following a megathrust earthquake, and then decrease in time. This simple relaxation of post-seismic creep rates is consistent with most observations following megathrust earthquakes (e.g. Miyazaki *et al.* 2004; Hsu *et al.* 2006; Chlieh *et al.* 2007). Depending on the amount of cumulative post-seismic creep, creep rates late in the seismic cycle may be substantially lower than plate rate. These low creep rates can be simply understood by appealing to the creep budget required to satisfy the long-term plate convergence rate, where heightened post-seismic creep rates are offset by low creep rates late in the seismic cycle. In other words, interseismic creep rates late in a cycle reflect the deficit between all creep during the cycle and the earthquake slip needed to account for the plate convergence. In our model, the decrease of creep rates during the interseismic period are due to a decrease of traction surrounding the asperities as the coseismic stresses are relaxed, and in essence, asperities mechanically shadow the surrounding fault during the later interseismic period. The degree to which the asperities shadow stresses depends on both the megathrust rheology and the geometry of the asperities. We consider both RD and RS friction megathrusts. We first explore the effect of the megathrust rheologies, and then the effect of the shape and distributions of the asperities. We do not attempt to explore the infinite

range of model rheologies or geometries, instead we present a few models in order to illustrate the connection between post-seismic transient creep and stress shadows.

4.1 Megathrust rheology

4.1.1 Rate-dependent friction

In the case of an RD frictional megathrust, as α'_h decreases, post-seismic creep is activated over a larger region of the megathrust surrounding the asperity (Fig. 4). When $\alpha'_h = 0.02$, there is significant post-seismic creep updip of the asperity, as well as over a broad region surrounding the asperity (Fig. 4a). These regions of heightened post-seismic creep roughly correlate with low creep rates at the end of the interseismic period (Fig. 4d). As α'_h increases, post-seismic creep is more localized near the asperity and there is less total post-seismic creep (Figs 4b and c). Hence, for larger α'_h, the stress shadow is smaller around the asperity later in the interseismic period (Figs 4e and f). We can quantify the relation between the coseismic slip and the stress shadow by the ratio of the potency of the late interseismic slip deficit [defined by $(1 - v')$ times area, which we refer to simply as the potency of the stress shadow] to the potency of the coseismic slip (coseismic slip times area). In these three models, the potency of the stress shadow is roughly five, three and two times the coseismic potency, for $\alpha'_h = 0.02$, 0.10 and 0.40, respectively. With an RD friction fault, the late interseismic stress shadow roughly correlates with the regions over which transient post-seismic creep is activated.

4.1.2 Rate- and state-dependent friction

In the case of an RS frictional megathrust, decreasing α' results in post-seismic creep activated over larger regions of the megathrust surrounding the asperity, similar to models with RD frictional faults (Figs 5a–c). Although, compared to RD friction models, the heightened post-seismic creep rates in RS friction models last longer into the interseismic period, because transient post-seismic creep can propagate from the asperities as fairly long-lived creep pulses (see Paper I). These post-seismic creep pulses increase the total transient creep in the regions farther from the asperity, regions that did not experience heightened post-seismic creep rates immediately following the earthquake. As a result, unlike the RD friction models, the stress shadows on RS frictional faults that develop around asperities are significantly larger than the regions experiencing immediate short term post-seismic creep (Figs 5d–f). In these models, the potency of the stress shadows is about three to six times the potency of the coseismic slip.

Changes in L' strongly affect the spatio-temporal pattern of post-seismic creep (see Paper I). In models we explored but do not present here, the stress shadows that developed late in the interseismic period were all similar for various L'. Due to computational limits, we were unable to explore models with L' less than 0.01, and

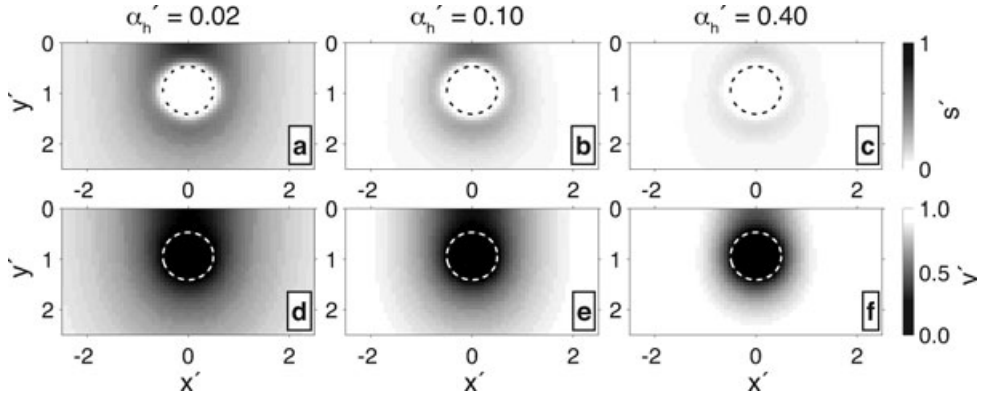

Figure 4. RD friction models: (a)–(c) Cumulative post-seismic creep in the first $t' = 0.05$ following the coseismic slip in Fig. 2(a), for models with RD frictional megathrusts ($\rho_h = 10$ and α'_h as indicated). (d)–(f) Corresponding interseismic creep rate immediately prior to the next earthquake in a seismic cycle. Asperity is denoted by dashed line, surface projection of the fault is shown.

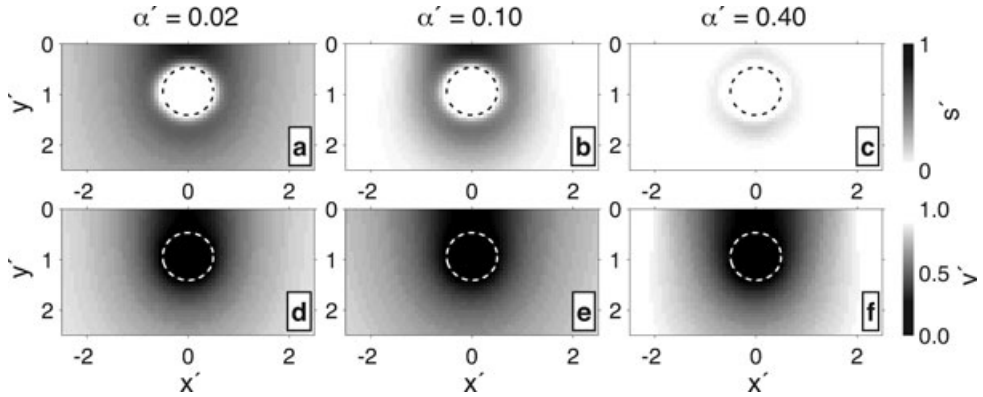

Figure 5. RS friction models: Cumulative post-seismic creep in the first $t' = 0.05$ of a seismic cycle (a–c), and corresponding interseismic creep rate immediately prior to the next earthquake (d–f), for models with RS frictional megathrusts ($\rho = 10$, $\gamma = 0.9$, $L'_o = 0.06$, and α' as indicated); the coseismic slip is shown in Fig. 2(a), dashed line indicates the asperities, and surface projection of the fault is shown.

the largest L' we considered was 0.30. For coseismic slip of 1 m, $L' = 0.01$ corresponds to $L = 1$ cm, significantly larger than the experimentally derived $L = 10^{-6}$ to 10^{-4} m (e.g. Marone 1998). Marone & Kilgore (1993) suggested that L may be of order 1 cm in natural faults, although Lapusta & Rice (2003) argued that the experimentally observed values are more appropriate for natural faults. The post-seismic creep pulse in 2-D models with $L' < 0.01$ propagate from the asperity at a faster rate, and thus there is more cumulative creep immediately after the earthquake and farther from the asperity (Paper I).

During the second half of the interseismic period there is a slight increase of creep rates near the asperity, and thus an erosion of the stress shadow (the effect is strongest for low α'). The increase of the creep rates does not appear to be due to a limited computational domain (as described in Section 3.3 of Paper I), rather it appears that the increase of L' in the far-field is the cause of this increase in creep rates. These far-field regions slide close to v_T throughout the interseismic period, although the creep rate varies in response to slip on the rest of the fault. On the other hand, if the computational domain was smaller, it would be assumed that these far-field regions slide at the fault loading rate regardless of slip elsewhere on the fault. The effect on the creep rate near the asperity is much less pronounced with a large fault domain and large far-field L', compared to a limited fault domain size. In these models, after the coseismic stresses have decayed around the asperities, the stresses due to the far-field creep cause a slight increase (less than about 5 per cent) in the creep rates near the asperities.

4.1.3 Comparison of rate-dependent and rate- and state-dependent friction

As illustrated in Paper I and in Perfettini & Ampuero (2008), models with RD or RS friction predict similar creep rates later in the interseismic period as long as $\alpha_h = \alpha(1 - \gamma)$ and $\rho_h = \rho/(1 - \gamma)$. In these models, we compare frictional models for $\rho_h = \rho = 10$ and $\alpha_h = \alpha$. Our purpose here is not to investigate when creep in models with RS friction is similar to that in models with RD friction; rather we are concerned with comparing models which have either a similar amount of post-seismic creep at a given time, or a similar stress shadow later in the interseismic period.

In Fig. 6, we show the cumulative creep at three times in the early interseismic period, and creep rates at three times in the late interseismic period. For simplicity, we only present the creep and creep rates along the centre line ($x = 0$) of the models. The cumulative creep at any time during the interseismic period is different in models with either RD or RS friction and $\alpha_h = \alpha = 0.02$, although the difference is not large (Fig. 6a). The interseismic creep rates in these two models are quite similar, and are fairly constant during the second half of the interseismic period (Fig. 6c). In models with either RD or RS friction and $\alpha_h = \alpha = 0.4$, the cumulative creep is only similar at $t' = 0.05$ (Fig. 6b). There is more cumulative creep in the model with RS friction in later times compared to models with RD friction, as the heightened post-seismic creep rates propagate farther from the asperity. Similarly, the creep rates later in the interseismic period are significantly distinct in these two models (Fig. 6d). Lower creep rates late in the interseismic period reflect both coseismic slip and any transient creep at any time during the interseismic period. Compared to in the RD friction model, with RS friction, there may be more transient creep farther from the asperity and continuing later into the seismic cycle.

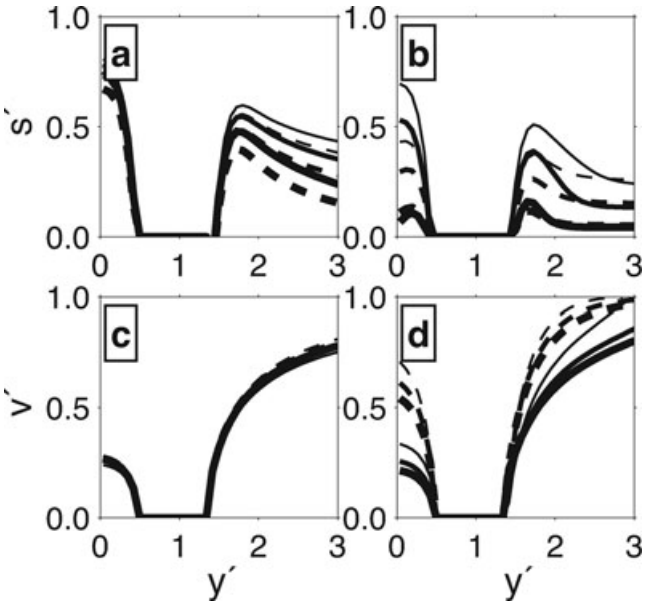

Figure 6. (a)–(b) Cumulative creep along $x' = 0$ at three times in models with RD (dashed lines; $\rho_h = 10$) or RS (solid lines; $\rho = 10$, $\gamma = 0.9$, and $L'_o = 0.06$) friction, and $\alpha_h = \alpha = 0.02$ (a) or 0.40 (b); creep is shown at $t' = 0.05$ (thick lines), 0.15 (medium lines), and 0.25 (thin lines). (c)–(d) Corresponding interseismic creep rate along $x' = 0$ at three times in the models with RD (solid lines) or RS (dashed lines) friction; creep rates are shown at $t' = 0.6$ (thin lines), 0.8 (medium lines) and immediately before the next earthquake (thick lines).

4.2 Asperity geometry

In Fig. 7, we show the creep rates late in a seismic cycle for three different asperity geometries and an RS frictional fault. In all models, the coseismic slip is constant over the asperity, and tapers into the surrounding fault to a similar degree as the above circular asperities (Figs 2a and b). Compared to the circular asperities, when the asperity either extends farther downdip or is longer along strike, it is more effective at creating a stress shadow late in the interseismic period (Figs 5e and 7). The stress shadow is more pronounced updip of the asperity as a result of greater post-seismic creep near the free-surface. In other words, larger asperities mechanically isolate the updip regions from the stable creep in the far-field. As a result, asperities that are longer along strike produce larger stress shadows relative to the coseismic potency. In addition, the stress shadows around deeper asperities are larger relative to the coseismic potency than those around shallow asperities, due to the larger updip regions that are shadowed (Figs 7b and c).

4.3 Multiple asperities

Multiple asperities can act together to shadow stresses over a larger region than the linear superposition of the stress shadows from the individual asperities. To illustrate stress shadows for multiple asperities, we consider two configurations of asperities: first two asperities of equal size, and second a large asperity surrounded by several small asperities.

4.3.1 Two equal sized asperities

We first consider a model with two circular asperities, with coseismic slip in Fig. 2(a), separated by a variable distance. We impose

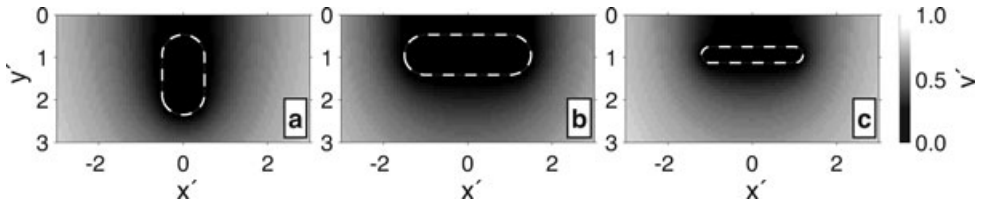

Figure 7. Interseismic creep rate immediately prior to an earthquake in a seismic cycle, in models with an RS frictional fault ($\rho = 10$, $\gamma = 0.9$, $L'_o = 0.06$ and $\alpha' = 0.1$); dashed line indicates the asperities, and surface projection of the fault is shown.

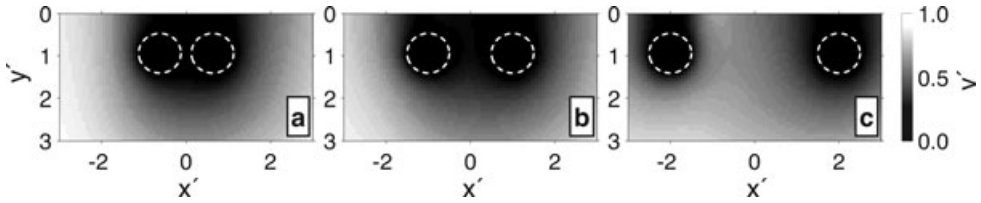

Figure 8. Interseismic creep rate immediately prior to an earthquake on the left-hand asperity, in models with an RS frictional fault ($\rho = 10$, $\gamma = 0.9$, $L'_o = 0.06$ and $\alpha' = 0.1$); dashed line indicates the asperities, and surface projection of the fault is shown.

coseismic slip on the two asperities periodically, each with maximum slip s_o and repeat time T, such that each asperity slips $T/2$ after the adjacent asperity (i.e. the earthquakes on the two asperities alternate). We refer to the asperity at $x < 0$ ($x > 0$) as the left (right) asperity. In Fig. 8, we show the interseismic creep rates before the earthquake of the left asperity. When the asperities are close together, there is a large stress shadow surrounding the asperities, that is of comparable size to a stress shadow around a continuous asperity of the same dimensions (Figs 7b and 8). Hence, late in a seismic cycle, the region between the two asperities would appear almost fully coupled in a backslip model, and may be difficult to distinguish from a single asperity in practice. When the asperities are farther apart, the stress shadows around each asperity are more similar to those around isolated asperities, with the region between the asperities creeping closer to the plate rate late in the interseismic period (Fig. 8c).

In the two asperity models we show, the stress shadows are asymmetric late in the interseismic period, and are slightly stronger surrounding the asperity that is not about to slip (the right asperity; Fig. 8a). This seems counter-intuitive, since one would expect that the stress shadow would be larger around the asperity that is about to slip (the left asperity). The weaker stress shadow around the left asperity is partly due to the influence of the far-field increase in L', as described in Section 4.2; however, the erosion of the left stress shadow is mostly due to an increase in creep rates caused by the propagation of a long-lived post-seismic creep pulse from the right asperity. In these models, we assumed an RS frictional rheology with a fairly large L' of 0.06. As a result, there is a fairly broad and long-lived post-seismic creep pulse which propagates from the asperity following an earthquake. When the post-seismic creep pulse encounters the adjacent asperity, it propagates at a slightly slower rate, and thus the relaxation of the post-seismic traction continues late into the seismic cycle. Hence, post-seismic creep from the right asperity increases the creep rates around the left asperity, thereby eroding the stress shadow around it.

4.3.2 One large asperity surrounded by multiple small asperities

We next consider a model with one circular asperity surrounded by 30 smaller asperities (Fig. 9a). We make no assumption of the velocity weakening frictional parameters of the asperities, rather we impose that all of the small asperities slip together, either with slip s_o and at the same time as the main asperity, or with slip $s_o/10$ and periodically ten times as often as the main asperity. We apply uniform slip within the small asperities, and do not taper the coseismic slip outside of the small asperities. We refer to the model in which all of the small asperities coseismically slip with the main asperity as the 'aftershock model'. The aftershock model is motivated by the elastodynamic model of Kato (2006), which includes small velocity weakening regions surrounding a large velocity weakening asperity. In his model, aftershocks on the small velocity weakening regions are caused by post-seismic creep following the main earthquake. In our aftershock model, all asperities rupture at once, and so we assume that the length of the aftershock sequence is short compared

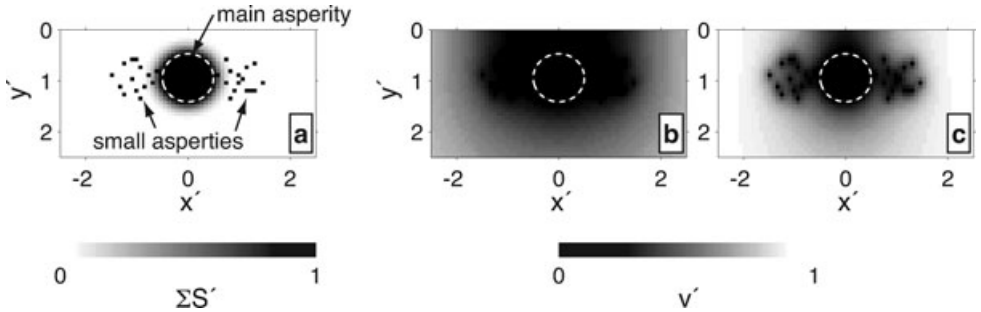

Figure 9. (a) Megathrust model with one main asperity and 30 small asperities, cumulative imposed coseismic slip over one seismic cycle, $\Sigma S'$, is shown in grey-scale, and the white dashed line outlines the main asperity. (b)–(c) Creep rate prior to the next earthquake on the main asperity, in the aftershock model (b) or repeater model (c). The fault in both models is RS friction, with $\rho = 10$, $\gamma = 0.9$, $L'_o = 0.04$ and $\alpha' = 0.1$, in both models.

to the interseismic period and that the cumulative coseismic slip in the aftershock sequence equals the coseismic slip of the main asperity. The second model, which we refer to it as the 'repeater model', is roughly analogous to a series of isolated asperities which rupture regularly during the interseismic period. Although highly idealized, the repeater model is motivated by the repeating earthquakes on the Japan trench investigated by Igarashi *et al.* (2003).

As mentioned above, the details of coseismic slip depend not only on the velocity weakening frictional parameters, but also on the heterogeneous velocity strengthening frictional parameters surrounding the asperities (e.g. Boatwright & Cocco 1996; Tinti *et al.* 2005; Hillers & Wesnousky 2008). We assume that there exists some velocity weakening rheologies of the asperities and transition regions, such that the recurrence time and slip magnitude in an elastodynamic model would be similar to those assumed here. Chen & Lapusta (2009) showed that there may be significant aseismic creep on a small velocity weakening asperity surrounded by a velocity strengthening region, and thus by assuming that the small asperities do not creep during the interseismic, we might be overestimating the stress shadow effect. Hence, both of these models with small asperities might be better considered using elastodynamic models, that include both velocity weakening and strengthening rheologies. Nevertheless, we present these two models in order to illustrate two cases where earthquakes on small asperities affect stress shadows around large asperities late in the interseismic period.

In the aftershock model, late in the interseismic period the stress shadow is comparable in size to a stress shadow resulting from a much larger asperity (Figs 9b and 7b). In this model, the coseismic slip on the small asperities effectively increases the coseismic traction perturbation at a distance from the main asperity, and the increase in the total amount of transient post-seismic creep is directly related to the increase in the size of the stress shadow. In the repeater model, the stress shadow at the end of the interseismic period is also larger, although much rougher, than the stress shadow that would result if the main asperity were isolated (Figs 9c and 5). The lower coseismic slip and shorter period of the earthquakes on the small asperities in the repeater model, cause transient coseismic traction perturbations to persist throughout the interseismic period, and thus the stress shadow is less pronounced compared to the aftershock model.

Given the regularization imposed in conventional backslip models, the roughness of the stress shadow in the repeater model may not be detectable. Decreasing the number of small asperities will decrease the effectiveness of the interseismic stress shadow, since the creep rates between the small asperities will be slightly larger at the end of the interseismic period. In general, multiple small asperities near a larger asperity will always result in a larger stress shadow than the larger single asperity will produce. Due to the fact that we are imposing coseismic slip, and not solving for it in an elastodynamic model, we may be over estimating the stress shadow effect. However, it is important to note that unless the fault boundaries are far enough from the asperities, elastodynamic models may underestimate late interseismic stress shadows, since the interseismic creep rates may be artificially raised due to the proximity of the boundary conditions.

5 TRANSIENT CREEP AND MEGATHRUST RHEOLOGY

In this section, we first explore some salient features of interseismic creep for various frictional parameters. In these models, the frictional parameters are again heterogeneous across the entire megathrust, but are homogeneous in the vicinity of the asperities (Fig. 1b). The far-field heterogeneity modifies the interseismic creep slightly, for instance by limiting the extent of transient post-seismic creep or increasing the creep rates near the asperities later in the interseismic period. Heterogeneous frictional parameters close to the asperities affect the interseismic creep to a much larger degree than far-field heterogeneity, and we also present a demonstration model with heterogeneous frictional parameters near the asperities.

We consider models with a single asperity with broadly tapered coseismic slip outside of the asperity (Fig. 2c), and only present the cycle-invariant results of fully spun-up models. Coseismic slip in elastodynamic models depends on both the velocity weakening frictional parameters within the asperities, as well as on the frictional parameters in the transition regions surrounding the asperities (e.g. Boatwright & Cocco 1996; Tinti *et al.* 2005; Hillers & Wesnousky 2008). In these models, we impose coseismic slip, and solve for interseismic creep outside the asperity, and thus the imposed coseismic slip in the transition regions is not necessarily consistent with the the velocity strengthening frictional rheology assumed adjacent to the asperity. Nevertheless, in order to illustrate several possible features of transient creep following large earthquakes, we impose broadly tapered coseismic slip so that the coseismic traction perturbation extends over a broad region of the fault. These broad perturbations exaggerate the effects we explore; however, the general features we discuss are similar to those in models with other imposed coseismic slip in transition regions, which we discuss below. We do not consider any coseismic change in θ' in the regions of coseismic slip, and we remark on this in the Discussion section.

In Fig. 10, we show the interseismic creep rates along the surface and downdip of the asperity in models with varying α' and $L'_{\rm o}$, assuming homogeneous α' and the heterogeneous L' shown in Fig. 1(b). With low $L'_{\rm o}$ and α', there is more transient post-seismic creep, and fairly strong post-seismic creep pulses propagate from the asperities throughout the early interseismic period (Figs 10a and e). Increasing $L'_{\rm o}$ greatly reduces the spatial size and duration of the creep pulses. For instance, when $L'_{\rm o} = 0.04$ and $\alpha' = 0.06$ there is a fairly substantial creep pulse during the first several percent of the interseismic period, with creep rates two to four times plate rate at the free surface and 10–20 times plate rate at depth (Figs 10a and e). Increasing $L'_{\rm o}$ to 0.14 results is a much smaller, almost negligible, creep pulse that propagates along the surface (Figs 10b and f). With RS friction and large α', the initial post-seismic creep is inhibited, but the fault eventually weakens and the creep rates increase. Increasing α' from 0.06 to 0.40, with $L'_{\rm o} = 0.04$, the immediate post-seismic creep rates are drastically decreased, although the creep rates slowly increase to several times plate rate later in the interseismic period (Figs 10c and g). With large $L'_{\rm o}$ and α', the interseismic creep is more steady during the interseismic period (Figs 10d and h).

These models illustrate the two fundamental modes of transient creep following earthquakes we see in these models. In the first, post-seismic creep is initially large and then decays through time, either with or without a pronounced creep pulse. In the second, post-seismic creep is delayed as creep rates are initially low after the earthquake and then increase in time. In the latter case, the heightened transient creep rates may occur well into the interseismic period, and last a significant time span. We refer to this mode of transient creep as 'delayed post-seismic creep'. There is a complicated dependence between the frictional parameters in which delayed post-seismic creep is favoured in these models, and the assumed coseismic slip and heterogeneous frictional properties. In

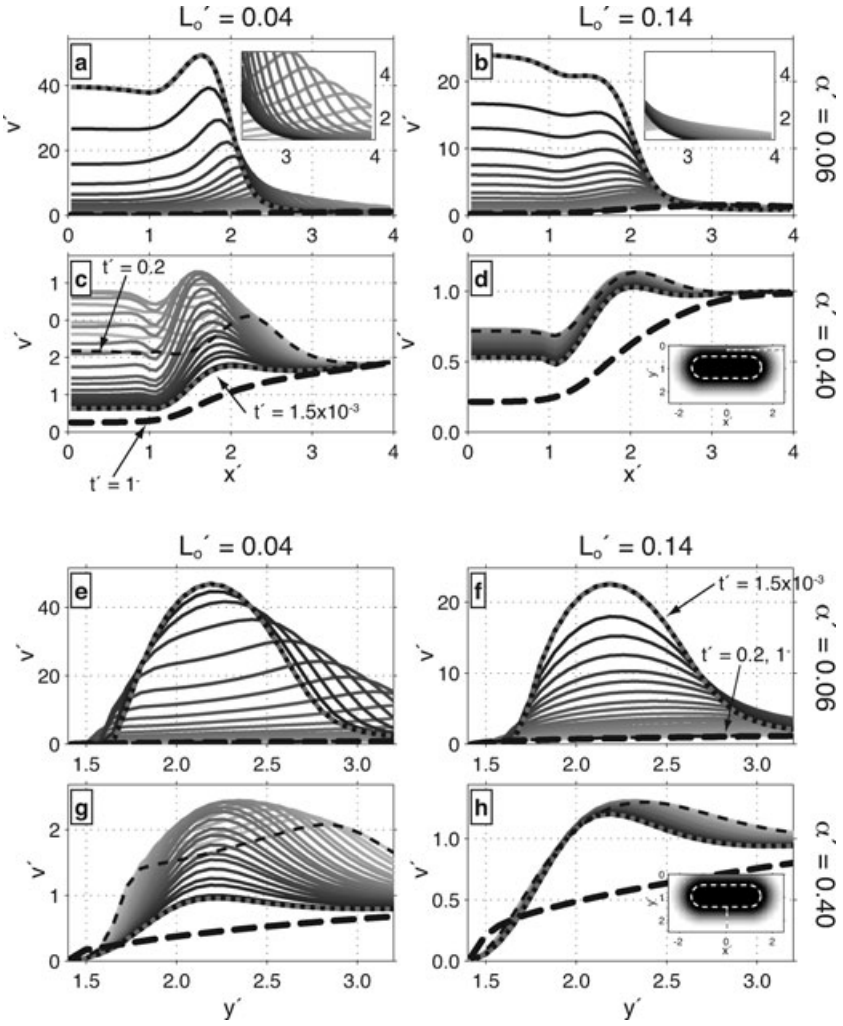

Figure 10. Interseismic creep rates along the surface (a)–(d) (inset in (d) shows profile location relative to coseismic slip) and down dip of the asperity (e)–(h) (inset in (h) shows profile location), at $t' = 0.0015$ (black-grey stippled line), $t' = 0.2$ (black thin dashed line), and at the end of the seismic cycle ($t' = 1^-$, black thick dashed line). Dark to light solid lines are the creep rates every 20th time step between $t' = 0.0015$ and 0.2 (note that due to the non-linear time-stepping in the model, these lines are not evenly spaced in model time, and are only shown to give an indication of the variation through time). $L'_o = 0.04$ in the models shown in the left-hand panels and 0.14 in the right-hand panels, $\alpha' = 0.06$ in (a, b, e, and f), and 0.40 in the remaining panels. Insets in (a) and (b) is a blow-up of the creep rates for $x' = 2.5$–4.0, axes labels are not shown for simplicity.

general, for the coseismic slip in Fig. 2(c), delayed post-seismic creep occurs in regions downdip of the coseismic slip for α' greater than about 0.1. As L' increases, delayed post-seismic creep only occurs for slightly larger α'. The exact frictional parameters needed for delayed post-seismic creep to occur also depend on the details of the imposed coseismic slip. For instance, using the more compact coseismic slip in Fig. 2(b), delayed post-seismic creep occurs for α' greater than about 0.3, although the delayed post-seismic creep is less pronounced. Finally, delayed post-seismic creep is only favoured in models with near-field heterogeneous α' when a region of elevated α' is close to, and is of comparable size to, the asperity. When the region of elevated α' decreases in spatial size, delayed post-seismic creep is only favoured at larger α'.

To illustrate interseismic creep in a model with heterogeneous RS frictional parameters near the asperity, we construct a model using the coseismic slip in Fig. 2(c). We increase α' to five times the background value, α'_o, in a broad region downdip of the asperity (Fig. 11a). Recalling that $\alpha' = a\sigma'_E$, we can interpret the increase of α' to be the result of either an increase in the magnitude of the frictional direct effect or a larger effective normal traction across the megathrust; for simplicity we refer to the region of increased α' as the 'clamped region'. We use the same far-field heterogeneous distribution of L' as in the previous model (Fig. 1b), but in the near-field we increase L' at the surface to five times the background value, L'_o (Fig. 11b). We increase α' downdip of the asperity to generate delayed post-seismic creep, and we increase L' near the surface, while keeping α' low, to avoid either delayed post-seismic creep or the propagation of large post-seismic creep pulses along the free surface. Assuming $\alpha'_o = 0.1$ and $L'_o = 0.04$, the creep rates updip of the asperity are large immediately following an earthquake (up to $v' = 40$), and then decrease below plate rate during the first several percent of the interseismic period (Figs 12a–d). In contrast to updip, there is negligible immediate post-seismic creep in the clamped region downdip of the asperity (Figs 12a–c). By about $t' = 0.04$, the creep rates at the downdip edge of the clamped region begin to increase, beginning an episode of delayed post-seismic creep that lasts about 20 per cent of the interseismic period (Figs 12c–f). The maximum creep rates in the delayed post-seismic creep are up to four times plate rate, and extend over a broad region downdip of the asperity.

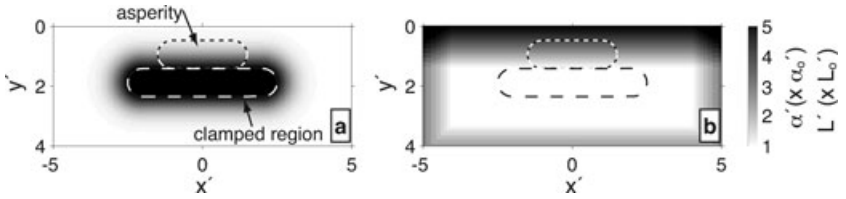

Figure 11. Surface projection of heterogeneous α' (a) and L' (b) in the demonstration megathrust model; grey-sale indicates α' (a) and L' (b) as a factor of α'_o and L'_o. Short dashed line demarcates the outline of the asperity, and long dashed line indicates the clamped region.

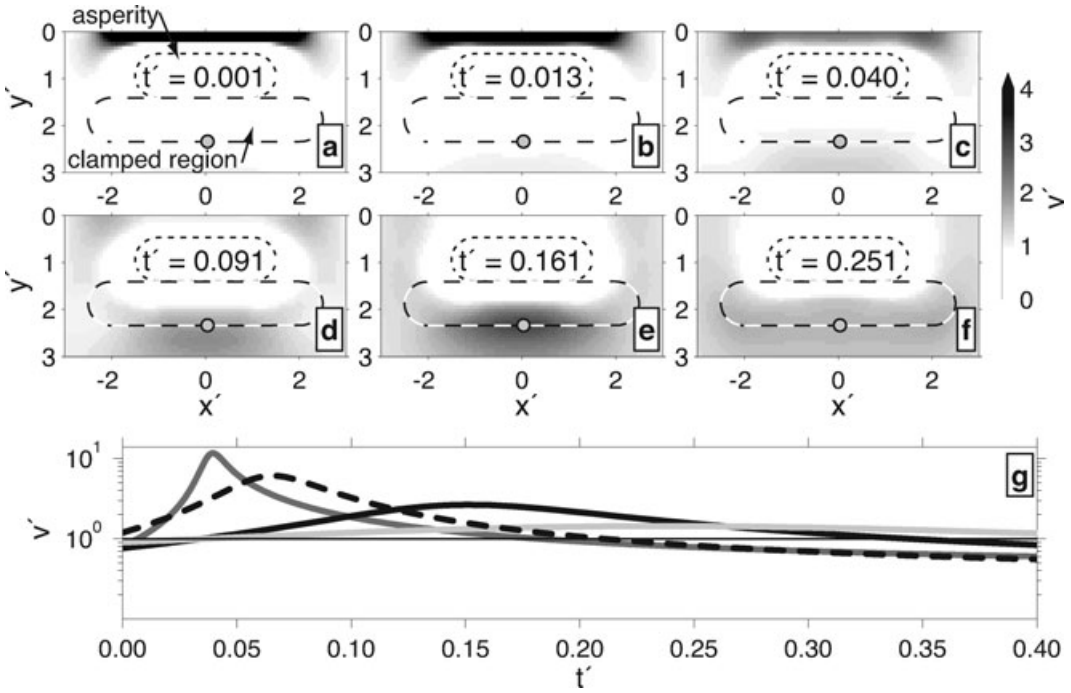

Figure 12. (a)–(f) Interseismic creep rate on the megathrust model in Fig. 11, at the indicated times and $\rho = 10$, $\gamma = 0.9$, $\alpha'_o = 0.1$ and $L'_o = 0.04$. Short dashed line demarcates the outline of the asperity, and long dashed line indicates the clamped region. (g) Interseismic creep rate at the location of the filled circle in panels (a–f) (thick black line), and the creep rate at the same location in models with $\alpha'_o = 0.05$ and $L'_o = 0.04$ (black dashed line), and $\alpha'_o = 0.1$ and $L'_o = 0.01$ (dark grey line) or 0.10 (light grey line). Thin black line indicates plate rate.

It is useful to consider the delayed post-seismic creep observed in these models in light of the condition for unstable transient creep determined by Perfettini & Ampuero (2008). They found that on a velocity strengthening RS friction fault, transient creep will become unstable following a traction perturbation as long as the characteristic size of the traction perturbation is larger than $L'_b = L'/\gamma\alpha'$, where we have non-dimensionalized L_b by D and L by s_o (see also Paper I, Section 5.4; Perfettini & Ampuero 2008). Hence, for a given coseismic traction perturbation, by either lowering L' or increasing α' we get delayed post-seismic creep. (An increase in γ may also result in delayed post-seismic creep, noting that $\gamma < 1$ for velocity strengthening faults.) Setting $\alpha'_o = 0.1$, and decreasing L'_o from 0.1 to 0.01 in these models, the maximum post-seismic creep rates in the clamped region increase (Fig. 12g). In addition, with decreasing L' the maximum creep rates occur earlier, and the duration of delayed post-seismic creep is shorter. Decreasing α'_o also decreases the duration of, and increases the maximum creep rates in, the delayed post-seismic creep episode (Fig. 12g). Due to the fault cell size in these models, we do not explore lower values of L'. In 2-D models we have run with lower L', we find that the maximum creep rates in the delayed post-seismic creep can be up to several orders of magnitude above plate rate and occur much earlier in the interseismic period, similar to the unstable transient creep explored by Perfettini & Ampuero (2008).

6 DISCUSSION

Most researchers acknowledge that the regions of megathrusts that appear partially to fully coupled in the backslip model merely reflects the slip-deficit on the megathrust, and these coupled regions may be areas of either coseismic slip or transient creep (e.g. Thatcher & Rundle 1984; Savage 1995; Mazzotti *et al.* 2000; Nishimura *et al.* 2004; Bürgmann *et al.* 2005). Indeed, low creep rates surrounding coseismic slip has been seen in the earliest elastodynamic models of Rice (1993), and all elastodynamic models of megathrusts include the effects of stress-shadows around regions of large coseismic slip late in the interseismic period (e.g. Hori *et al.* 2004; Liu & Rice 2005; Kato 2008). However, the late-interseismic stress shadows in elastodynamic models may be understated, due to the relatively small size of the computational domain of those models. In Paper I, we show that when the fault over which creep is calculated is only moderately larger than the size of the asperities, late in the interseismic period the creep rates near the asperity are larger than if the

computational domain was bigger (see section 3.3 of Paper I). The model of Kato (2008) contained four asperities on a 2-D fault in an elastic whole space, and the two largest asperities were roughly 50 km in size and separated by less than 50 km; however, the edges of the computational fault in the model of Kato (2008) were roughly 50 km from the asperities. Although the study was focused on the earthquake process in velocity weakening regions, Kato (2008) did note a lowering of interseismic creep rates between asperities and that regions where the creep rate was low prior to the earthquake corresponded with transient post-seismic creep. The need to limit the fault size in elastodynamic models is driven by the computational demands of calculating the evolution of coseismic slip, and we do not imply that the size of the computational domain needs to be large in models that focus on seismic slip. However, when investigating slow creep later in the interseismic period, it is important to verify that the model boundary conditions are not adversely impacting this aseismic creep.

In these models, varying frictional parameters affects the interseismic creep near the surface and at depth in similar ways, although certain effects are often exaggerated updip of the asperity due to the free surface at the trench. For instance, with low L' a post-seismic creep pulse may propagate along the trench with creep rates many times the plate convergence rate. In addition, with increasing α' there may be significant delayed post-seismic creep near the trench, that lasts through a non-negligible amount of the interseismic period. Either of these phenomena would be fairly easy to detect geodetically, and to our knowledge, they are not typically observed near trenches following megathrust earthquakes. Instead, one commonly observes post-seismic creep updip of megathrust earthquakes that decays through time (e.g. Miyazaki *et al.* 2004; Hsu *et al.* 2006; Chlieh *et al.* 2007). This lack of delayed transient creep may indicate that RS friction is not an appropriate rheology near the trench, or it may indicate that L' is large and α' is small in RS friction near the trench. Indeed large L' near the trench may be plausible assuming that L' is inversely proportional to the degree of shear localization in faults (e.g. Marone & Scholz 1988; Marone & Saffer 2007), and deformation becomes less localized towards the trench. Low α' near the trench might reflect the low effective normal traction at these shallow depths.

In most of the models we present, we ignored the variation of fault normal traction throughout the seismic cycle. We justified this assumption by showing that including the variation of normal traction on a planar dipping fault mainly affects the magnitudes of the creep rates, and not the cumulative creep. However, as shown in Section 5, delayed post-seismic creep is favoured for large $\alpha' = a\sigma'_E$, and thus including time variable normal traction in the calculation of transient slip on non-planar megathrust geometries may affect the mode of post-seismic creep which occurs. For example, if the megathrust dip increases downdip of a megathrust earthquake, coseismic slip would tend to increase the normal traction on the downdip regions of the megathrust, and thus temporarily increasing α'. Such coseismic clamping of the megathrust could inhibit the immediate post-seismic creep downdip of the earthquake, and for an RS frictional fault, these downdip regions might eventually weaken and transient creep would occur. The maximum creep rates, the duration of transient creep, and the delay of heightened creep rates after the earthquake, all depend on the megathrust geometry, rheology and coseismic slip.

Liu & Rice (2005) demonstrated a rich behaviour of transient interseismic creep in RS frictional elastodynamic models. Both Perfettini & Ampuero (2008) and Helmstetter & Shaw (2009), respectively referred to as PA2008 and HS2009 hereafter, subsequently explored two main modes of creep in velocity strengthening RS frictional models: simple decay of creep rates following a perturbation, and a transient creep event which is delayed in time following the perturbation. While the latter is similar to the delayed post-seismic creep we discuss, as their models do not calculate transient creep in response to coseismic slip, we use 'transient creep event' to describe the delayed transient creep in their models. (HS2009 also explored velocity weakening frictional parameters, finding three modes of slip, simple decay of creep rates, a transient creep event, or an earthquake; however, we limit our discussion of their paper to the velocity strengthening cases.) PA2008 applied a Gaussian shaped traction perturbation onto a 2-D fault plane, and PA2008 found that a transient creep event occurred only when the length scale of the shear stress perturbation exceeded some critical value that depended on the frictional properties of the fault. In their spring-and-slider model, HS2009 showed that a transient creep event was only permissible when the stiffness of the model was below some critical stiffness, and this condition is roughly equivalent to that of PA2008 (Appendix A1). HS2009 also showed that a transient creep event will only occur when the initial instantaneous friction of the fault was larger than a critical value, f_a. Specifically, they found that $f > f_a$ to generate a transient creep event, whereas when $f < f_a$ the creep rates stably decayed in time. For our purposes, it is useful to state this additional criterion for transient creep events as

$$\Omega > \frac{1}{1 - k/k_b} > 1, \tag{4}$$

where k is the stiffness of the fault, and k_b is a critical stiffness (Appendix A2). PA2008 also noted that the fault needs to be well above steady state (i.e. $\Omega \gg 1$), for a transient creep event to occur.

In these models, we have ignored any possible coseismic change in the frictional state variable, θ', in regions of imposed coseismic slip. During seismic rupture, θ' can vary over many orders of magnitude (e.g. Ampuero & Rubin 2008), and immediately following coseismic slip, θ' may be as low as $\theta'_{\rm co} = L'/v'$. Taking 1 m s^{-1} to be a typical seismic rupture speed (e.g. Heaton 1990), and assuming $v_T = 3$ mm yr^{-1}, $\theta'_{\rm co} = L'/10^9$. This issue is also discussed in Paper I, Section 5.6, where we show that accounting for a coseismic change in θ', initial post-seismic creep rates are significantly higher than if a coseismic change in θ' was ignored. Accounting for a coseismic change in θ' will also affect the conditions in which delayed post-seismic creep is favoured. For instance, in most of the models discussed in Section 5, the coseismic shear stress perturbation overlaps regions that also slipped coseismically (see also Paper I, Section 3.2), and under the right frictional conditions, the regions that experience delayed post-seismic creep overlap regions of imposed coseismic slip. If $\theta' = \theta'_{\rm co}$ in transition regions immediately following coseismic slip, $\Omega = |v_{\rm post}|/|v_{\rm co}| \ll 1$, and the condition in eq. (4) will never be satisfied. In many of the models we have run, delayed post-seismic creep does not occur when we include such a drastic coseismic change in θ'. Delayed post-seismic creep does occur when we account for a coseismic change in θ' in the model in Figs 11 and 12, although the timing and creep rates of the delayed post-seismic creep are different. The reason that a coseismic drop in θ' does not change the mode of post-seismic creep in this model, is that the delayed post-seismic creep initiates at the downdip edge of the clamped region, and is away from the region of imposed coseismic slip and drop in θ'. Due to the complexity of the interaction between the coseismic slip, and the heterogeneous frictional properties, we do not attempt to establish quantitative conditions

necessary for transient post-seismic creep to be delayed. However, we point out that by only considering relatively simplified models, the conditions necessary for transient creep events to be caused directly by earthquake slip may be overstated.

7 CONCLUSIONS

In mechanical models with frictional faults, creep rates late in a seismic cycle reflect the deficit between the total slip expected over a seismic cycle, and the sum of coseismic slip and cumulative transient post-seismic creep (Savage 1983; Savage 1995). In other words, late in a seismic cycle the creep rates surrounding an asperity may be lower than plate rate if there was significant post-seismic creep in these regions. Hence, late in a seismic cycle, coupling inferred in a backslip model may not necessarily reflect the configuration of asperities or coeseismic slip, but only reflect the stress shadows surrounding those asperities. While this creep budget description of stress shadows is similar to that made in kinematic models (e.g. Savage 1983), in our model the lower creep rates around the asperities are due to the shadowing of stresses by the interseismically locked asperity. In elastodynamic models these late interseismic stress shadows may be understated, due to the limited computational domain in those models focused on the earthquake rupture process. The details of the stress shadows depends on the megathrust rheology, the configuration of asperities, and their histories of coseismic slip. For RD friction faults, the size of stress shadows increase as there is more transient post-seismic creep. For RS friction faults, there may be significant long-lived post-seismic creep at rates comparable to the plate convergence rate, and thus the amount of early post-seismic creep may not indicate the size of the later interseismic stress shadows.

We show that there is a wide range of transient post-seismic creep that may occur. In the standard conception of post-seismic creep, the creep rates following coseismic slip are initially high, and then decay during the interseismic period. However, for some RS frictional rheologies, post-seismic creep may be delayed, similar to the unstable transient creep documented by Perfettini & Ampuero (2008) and Helmstetter & Shaw (2009). In undelayed post-seismic creep, maximum creep rates decrease with time, but transient creep can continue in creep pulses that propagate from the asperities at rates comparable, or slightly lower, than plate rate well into the interseismic period. In delayed post-seismic creep, the immediate post-seismic creep rates following coseismic slip are low, but then increase at later times, only to eventually decrease back below the plate convergence rate. It is plausible that delayed post-seismic creep can initiate several years to decades after a megathrust earthquake, and last a substantial portion of the seismic cycle, and thus may not be readily recognized as transient post-seismic creep. Delayed post-seismic creep is generally favoured when $\alpha' = a\sigma'_E$ is large and the fault is above steady state following coseismic slip.

The dependence of interseismic creep on megathrust rheologies and asperity geometries can be complicated, but due to the relatively low computational cost of our model, many configurations of asperities, coseismic slip histories, and fault rheologies can be tested. It might be difficult to infer fault rheology from only observations of interseismic deformation late in the seismic cycle. However, one would likely be able to infer plausible asperity geometries from steady interseismic deformation. Additional observations of transient post-seismic creep would increase ones ability to constrain megathrust rheologies.

ACKNOWLEDGMENTS

We thank the editor, M. Cocco, and two anonymous reviewer for insightful comments and suggestions. We also thank R. Kanda for discussions that improved this manuscript. All calculations were done using Matlab, The Mathworks Inc. This research was supported in part by the Gordon and Betty Moore Foundation. This is Caltech Tectonic Observatory contribution #117 and Caltech Seismological Laboratory contribution #10,032.

REFERENCES

Aki, K., 1984. Asperities, barriers, characteristic earthquakes and strong motion prediction, *J. geophys. Res.,* **89,** 5867–5872.

Ampuero, J. & Rubin, A.M., 2008. Earthquake nucleation on rate and state faults—aging and slip laws, *J. geophys. Res.,* **113**(B1), doi:10.1029/2007JB005082.

Bilek, S. & Lay, T., 2002. Tsunami earthquakes possibly widespread manifestations of frictional conditional stability, *Geophys. Res. Let.,* **29,** 1673, doi:10.1029/2002GL015215.

Boatwright, J. & Cocco, M., 1996. Frictional constraints on crustal faulting. *J. geophys. Res.,* **101,** 13 895–13 909.

Bürgmann, R., Kogan, M.G., Steblov, G.M., Hilley, G., Levin, V.E. & Apel, E., 2005. Interseismic coupling and asperity distribution along the Kamchatka subduction zone, *J. geophys. Res.,* **110,** B07405, doi:10.1029/2005LB003648.

Chen, T. & Lapusta, N., 2009. Scaling of small repeating earthquakes explained by interaction of seismic and aseismic slip in a rate and state fault model, *J. geophys. Res.,* **114,** B01311, doi:10.1029/2008JB005749.

Chlieh, M. et al., 2007. Coseismic slip and afterslip of the great Mw 9.15 Sumatra-Andaman earthquake of 2004, *Bull. seism. Soc. Am.,* **97,** doi:10.1785/0120050631, S152–S173.

Chlieh, M., Avouac, J., Sieh, K., Natawidjaja, D.H. & Galetzka, J., 2008. Heterogeneous coupling of the Sumatran megathrust constrained by geodetic and paleogeodetic measurements, *J. geophys. Res.,* **113,** B05305, doi:10.1029/2007JB004981.

Dieterich, J., 1979. Modeling rock friction I: experimental results and constitutive equations, *J. geophys. Res.,* **84,** 2161–2168.

Fialko, Y., 2007. Fracture and frictional mechanics—theory, in *Treatise of Geophysics,* Vol. 4, pp. 83–106, ed. Kanamori, H., Earthquake Seismology, Academic Press, Elsevier, UK.

Hashimoto, C., Noda, A., Sagiya, T. & Matsu'ura, M., 2009. Interplate seismogenic zones along the Kuril—Japan trench inferred from GPS data inversion, *Nat. Geosci.,* **2,** doi:10.1038/ngeo421, 141–144.

Heaton, T., 1990. Evidence for and implications of self-healing pulses of slip in earthquake rupture, *Phys. Earth planet. Int.,* **64,** 1–20.

Heki, K., Miyazaki, S. & Tsuji, H., 1997. Silent fault slip following an interplate thrust earthquake at the Japan trench, *Nature,* **6625,** 595–597.

Helmstetter, A. & Shaw, B., 2009. Afterslip and aftershocks in the rate-and-state friction law, *J. geophys. Res.,* **114,** B01308, doi:10.1029/2007JB005077.

Hillers, G. & Wesnousky, S., 2008. Scaling relations of strike-slip earthquakes with different slip-rate-dependent properties at depth, *Bull. seism. Soc. Am.,* **98,** doi:10.1785/0120070200, 1085–1101.

Hori, T., Kato, N., Hirahara, K., Baba, T. & Kaneda, Y., 2004. A numerical simulation of earthquake cycles along the Nankai Trough in southwest Japan: lateral variation in frictional property dye to the slab geometry controls the nucleation position. *Earth planet. Sci. Lett,* **228,** 215–226.

Hsu, Y. et al., 2006. Frictional afterslip following the 2005 Nias-Simeulue earthquake, Sumatra, *Science,* **312,** doi:10.1029/2003JB002917, 1921–1926.

Igarashi, T., Matsuzawa, T. & Hasegawa, A., 2003. Repeating earthquakes and interplate aseismic slip in the northeastern Japan subduction zone, *J. geophys. Res.,* **108,** B5, doi:10.1029/2002JB001920.

Kanamori, H., 1986. Rupture process of subduction-zone earthquakes, *Ann. Rev. Earth planet. Sci.,* **14,** 293–322.
Kato, N., 2006. Expansion of aftershock areas caused by propagating post-seismic sliding, *Geophys. J. Int.,* **113,** 797–808, doi:10.1111/j.1365-246X.2006.03255.x.
Kato, N., 2008. Numerical simulation of recurrence of asperity rupture in the Sanriku region, northeastern Japan, *J. geophys. Res.,* **113,** B06302, doi:10.1029/2007JB005515.
Kanda, R.V.S. & Simons, M., 2009. A discussion of elastic dislocation models for interseismic deformation in subduction zones, *J. geophys. Res.,* in press, doi:10.1029/2009JB006611.
Lapusta, N. & Rice, J., 2003. Nucleation and early seismic propagation of small and large events in a crustal earthquake model, *J. geophys. Res.,* **108,** 2205, doi:10.1029/2001JB000793.
Liu, R. & Rice, J.R., 2005. Aseismic slip transients emerge spontaneously in three-dimensional rate and state modeling of subduction earthquake sequences. *J. geophys. Res.,* **110,** B08307, doi:10.1029/2-4JB003424.
Marone, C., 1998. Laboratory-derived friction laws and their application to seismic faulting, *Ann. Rev. Earth planet. Sci.,* **26,** 643–696.
Marone, C. & Kilgore, B., 1993. Scaling of the critical slip distance for seismic faulting with shear strain in fault zones, *Nature,* **362,** 618–621.
Marone, C. & Saffer, D., 2007. Fault friction and the upper transition from seismic to aseismic faulting, in *The Seismogenic Zone of Subduction Thrust Faults,* pp. 346–369, eds Dixon, T.H. & Moore, J.C., Columbia University Press, New York.
Marone, C. & Scholz, C., 1988. The depth of seismic faulting and the upper transition from stable to unstable slip regimes, *Geophys. Res. Lett.,* **15,** 621–624.
Marone, C., Scholz, C. & Bilham, R., 1991. On the mechanics of earthquake afterslip, *J. geophys. Res.,* **96,** 8441–8452.
Mazzotti, S., Pichon, X.L. & Henry, P., 2000. Full interseismic locking of the Nankai and Japan-west Kuril subduction zones: an analysis of uniform elastic strain accumulation in Japan constrained by permanent GPS, *J. geophys. Res.,* **105,** 13 177–13 177.
Meade, B.J. & Loveless, J.P., 2009. Predicting the geodetic signature of $M_W \geq 8$ slow slip events, *Geophys. Res. Lett.,* **36,** L01306, doi:10.1029/2008GL036364.
Miura, S., Iinuma, T., Tui, S., Uchida, N., Sato, T., Tachibana, K. & Hasegawa, A., 2006. Co- and post-seismic slip associated with the 2005 Miyagi-oki earthquake (M7.2) as inferred from GPS data, *Earth Planets Space,* **58,** 1567–1572.
Miyazaki, S., Segall, P., Fukuda, J. & Kato, T., 2004. Space time distribution of afterslip following the 2003 Tokachi-oki earthquake: implications for variations in fault zone frictional properties, *Geophys. Res. Lett.,* **31,** L06623, doi:10.1029/2003GL019410.
Nishimura, T., Hirasawa, T., Miyazaki, S., Sagiya, T., Tada, T., Miura, S. & Tanaka, K., 2004. Temporal change of interplate coupling in northeastern Japan during 1995–2002 estimated from continuous GPS observations, *Geophys. J. Int.,* **157,** doi:10.1111/j.1365-246X.2004.02159.x, 901–916.
Norabuena, E. *et al.*, 2004. Geodetic and seismic constraints on some seismogenic zone process in Costa Rica, *J. geophys. Res.,* **109,** B11403, doi:10.1029/2003JB002931.
Okada, Y., 1992. Internal deformation due to shear and tensile faults in a half-space, *Bull. seism. Soc. Am.,* **82,** 1018–1040.
Perfettini, H. & Ampuero, J., 2008. Dynamics of a velocity strengthening fault region: implications for slow earthquakes and postseismic slip, *J. geophys. Res.,* **113,** B09317, doi:10.1029/2007JB005398.
Pritchard, M.E. & Simons, M., 2006. An aseismic slip pulse in northern Chile and along-strike variations in seismogenic behavior, *J. geophys. Res.,* **111,** B08405, doi:10.1029/2006JB004258.
Rice, J., 1993. Spatio-temporal complexity of slip on a fault, *J. geophys. Res.,* **98,** 9885–9907.
Ruina, A., 1983. Slip instability and state variable friction laws, *J. geophys. Res.,* **88,** 10 359–10 370.
Savage, J., 1983. A dislocation model of strain accumulation and release at a subduction zone, *J. geophys. Res.,* **88,** 4984–4996.
Savage, J., 1995. Interseismic uplift at the Nankai subduction zone, southwest Japan, 1951–1990, *J. geophys. Res.,* **100,** 6339–6350.
Savage, J.C. & Burford, R.O., 1973. Geodetic determination of relative plate motion in central California, *J. geophys. Res.,* **78,** 832–845.
Suwa, Y., Miura, S., Hasegawa, A., Sato, T. & Tachibana, K., 2006. Interplate coupling beneath NE Japan inferred from three-dimensional displacement field, *J. geophys. Res.,* **111,** B04402, doi:10.1029/2004JB003203.
Thatcher, W. & Rundle, J.B., 1984. A viscoelastic coupling model for cyclic deformation due to periodically repeated earthquakes at subduction zones, *J. geophys. Res.,* **89,** 7631–7640.
Tinti, E., Bizzarri, A. & Cocco, M., 2005. Modeling the dynamic rupture propagation on heterogeneous faults with rate- and state-dependent friction, *Ann. Gephys.,* **48,** 327–345.
Wang, K., 2007. Elastic and viscoelastic models of crustal deformation in subduction earthquake cycle, in *The Seismogenic Zone of Subduction Thrust Faults,* pp. 540–575, eds Dixon, T.H. & Moore, J.C., Columbia University Press, New York.
Wang, K. & Dixon, T., 2004. "Coupling" semantics and science in earthquake research, *EOS, Trans. Am. geophys. Un.,* **85,** 181–182.
Wang, K. & He, J., 2008. Effects of frictional behavior and geometry of subduction fault on coseismic seafloor deformation, *Bull. seism. Soc. Am.,* **98,** doi:10.1785/0120070097, 571–579.
Yagi, Y., Kikuchi, M. & Nishimura, T., 2003. Co-seismic slip, post-seismic slip, and largest aftershock associated with the 1994 Sanriku-haruka-oki, Japan, earthquake, *Geophys. Res. Lett.,* **30,** 2177, doi:10.1029/2003GL018189.

APPENDIX A: CRITERIA FOR UNSTABLE CREEP

Perfettini & Ampuero (2008; PA2008) and Helmstetter & Shaw (2009; HS2009) determined conditions necessary for unstable transient creep in velocity strengthening RS frictional models. PA2008 determined that for unstable transient creep to be favoured in their 2-D models, the spatial size of a traction perturbation on a fault had to be larger than some critical size, and that the fault had to be above steady-state. In their spring-and-slider model, HS2009 determined that for transient creep to be unstable, the model stiffness had to be less than a critical value, and that the initial friction had to be larger than a critical value. In this appendix, we demonstrate an equivalence between the conditions of PA2008 and HS2009, and we derive a form of HS2009's second criteria that is used in Section 6.

A1 First criterion

PA2008 demonstrated that only when the length scale of shear stress perturbations, L_τ (see Table A1 for list of model symbols used in the Appendix), is greater than a critical length scale, L_b, does creep on velocity strengthening RS faults become unstable, creating a transient, aseismic slip event.

$$L_b = \frac{\mu L}{b\sigma_E}, \tag{A1}$$

and thus for unstable transient creep, PA2008 proposed that

$$L_\tau \gg \frac{\mu L}{b\sigma_E}. \tag{A2}$$

HS2009 found that the stiffness of their spring-and-slider model, k, needed to be less than a critical stiffness, k_b, for unstable transient creep

$$k_b = \frac{b\sigma_E}{L}. \tag{A3}$$

For a 2-D fault, we assume that the relevant stiffness is

$$k \approx \mu / L_{\mathrm{UTC}} \tag{A4}$$

Table A1. Definition of symbols used in the Appendix.

$f_{\rm ss}$	Steady-state fault friction
$L_{\rm UTC}$	Spatial dimension of region of the fault undergoing unstable transient creep
$L'_{\rm UTC}$	$= L_{\rm UTC}/D$
L_τ	Spatial dimension of coseismic traction perturbations on the fault

(e.g. Fialko 2007), and take $L_{\rm UTC}$ to be the spatial size of the region of the fault undergoing unstable transient creep. Therefore, we can express the first criterion of HS2009 as

$$\frac{\mu}{L_{\rm UTC}} < \frac{b\sigma_E}{L}. \tag{A5}$$

Assuming that $L_{\rm UTC} \sim L_\tau$ (i.e. the size of the regions of the fault undergoing unstable transient creep is comparable to the size of the shear stress perturbation), eq. (A5) can be written as

$$L_\tau > \frac{\mu L}{b\sigma_E}, \tag{A6}$$

demonstrating that conditions (A2) and (A5) are roughly equivalent in this case.

A2 Second criterion

The second criterion for unstable transient creep proposed by HS2009, is that the initial instantaneous friction, f, must be larger than a critical value, f_a, given by

$$f_a = f_{\rm ss} - b \ln\left(1 - \frac{k}{k_b}\right), \tag{A7}$$

where $f_{\rm ss}$ is the steady-state friction. f derived by HS2009 as

$$f = f_{\rm ss} + b \ln\left(1 - \dot{\theta}\right), \tag{A8}$$

and using eq. (3), the second criterion proposed by HS2009 can be expressed as

$$\Omega > \frac{1}{1 - k/k_b} > 1. \tag{A9}$$

In condition (A9) we also make use of the fact that $k < k_b$ must be satisfied for transient creep to be unstable, and the second condition of PA2008 is satisfied by eq. (A9). Using eqs (A3) and (A4) and the assumption that $L_{\rm UTC} \sim L_\tau$, we find

$$\frac{k}{k_b} = \frac{L}{L_{\rm UTC}} \frac{\mu}{b\sigma_E} = \frac{L'}{L'_{\rm UTC}} \frac{1}{\gamma\alpha'}, \tag{A10}$$

where $L'_{\rm UTC} = L_{\rm UTC}/D$.